AIP | Journal of Applied Physics

Band gap energies of solar micro/meso-porous composites of zinc (hydr)oxide with graphite oxides

SM Z. Islam, Taposh Gayen, Mykola Seredych, Oluwaniyi Mabayoje, Lingyan Shi et al.

Citation: J. Appl. Phys. **114**, 043522 (2013); doi: 10.1063/1.4816779
View online: http://dx.doi.org/10.1063/1.4816779
View Table of Contents: http://jap.aip.org/resource/1/JAPIAU/v114/i4
Published by the AIP Publishing LLC.

Band gap energies of solar micro/meso-porous composites of zinc (hydr)oxide with graphite oxides

SM Z. Islam,[1,2] Taposh Gayen,[2] Mykola Seredych,[3] Oluwaniyi Mabayoje,[3] Lingyan Shi,[4] Teresa J. Bandosz,[3] and Robert R. Alfano[1,2,a)]

[1]*Department of Electrical Engineering, The City College of New York, 160 Convent Ave, New York, New York 10031, USA*
[2]*Institute of Ultrafast Spectroscopy and Lasers, Departments of Physics and Electrical Engineering, The City College of New York, 160 Convent Ave, New York, New York 10031, USA*
[3]*Department of Chemistry, The City College of New York, 160 Convent Ave, New York, New York 10031, USA*
[4]*Department of Biomedical Engineering, The City College of New York, 160 Convent Ave, New York, New York 10031, USA*

(Received 1 May 2013; accepted 11 July 2013; published online 31 July 2013)

The band gap energies of micro/meso-porous zinc (hydr)oxide and its composites with 2 wt. % and 5 wt. % graphite oxides are reported using three optical characterization techniques. The obtained energy gaps (from 2.84 eV to 2.95 eV) of the composites are smaller than that for zinc oxide (~3.2 eV) and zinc (hydr)oxide (~3.06 eV). The band gap narrowing of the composite materials is due to the presence of defects, larger particle size, and weaker confinement. The bonds between zinc (hydr)oxide lattice and the carbon of graphene phase also contribute to this phenomenon. The structural properties of these materials are presented using Transmission Electron Microscopy, Scanning Tunneling Electron Microscopy, X-Ray analysis, and Two-Photon Fluorescence imaging Microscopy. © *2013 AIP Publishing LLC*. [http://dx.doi.org/10.1063/1.4816779]

I. INTRODUCTION

Amorphous micro/meso-porous materials are gaining importance in solar energy conversion and as sensors due to their low cost, high accessible surface area, and wide band gap energies.[1,2] As possible key components in solar converters and detectors, it is of great importance to determine band gap energies (i.e., direct gap energy, Urbach energy, etc.) and absorption coefficients of micro/meso-porous materials. A new class of micro/meso-porous material is zinc (hydr)oxide and its composites with graphite oxides (GO). Bandosz and co-workers[3] have shown that such materials exhibit the photo-activity in the visible light.[4–6] The determination of the optical band gap is important because it not only controls the efficiency for solar conversion and the shape of the optical emission spectrum but also manifests the effects of structural and thermal disorders on the electronic properties of the micro-composites.[7] The unique characteristics, such as improved structural[4–6] and electrical properties,[3,8] stem from the layered structure of the micro/meso-composites with chemically active oxygen groups at the basal planes of GO.[9] GO is found to be a promising material for a large scale graphene processing, as its chemical and thermal reductions are proven to produce a material with properties comparable to those of chemical vapor deposition (CVD)-grown graphene. The presence of increased GO phase in the final micro-composites formed is reported to increase electrical conductivity, and this feature is particularly important for energy storage and sensor applications.[3] These micron-sized pores can be filled with quantum dots and dye molecules to enhance conversion of energy from solar spectra.

In this paper, the energy gaps of porous zinc (hydr)oxide (referred to as $Zn(OH)_2$) and its composites with 2 wt. % and 5 wt. % graphite-oxide (GO) (referred to as ZnGO-2 and ZnGO-5, respectively) are determined and measured using three optical methods, such as, absorption spectroscopy, photoluminescence (PL) spectroscopy, and photocurrent experiment. The structural properties were determined by Transmission Electron Microscopy (TEM), Scanning Tunneling Electron Microscopy (STEM), X-Ray analysis, and Two-Photon Fluorescence (TPF) imaging techniques.

II. EXPERIMENTAL PROCEDURE

The samples were prepared by synthesis according to Refs. 3 and 6. GO was synthesized by oxidation of graphite (Sigma-Aldrich) using the Hummers method.[10] The composites were prepared by dispersing GO powder (2 wt. % or 5 wt. %) of the final mass of the material in 1.0 l zinc chloride solution (0.05M). The resulting well-dispersed suspension was stirred for 4 h. Sodium hydroxide solution (0.05M) was then added (2.0 l) with a rate of 2.0 ml min^{-1} using a Titronic Universal (SCHOTT) method. Afterwards, the obtained composites were extensively washed with distilled water until neutral pH and no traces of chloride ions were found. Finally, the suspension was centrifuged and a gel formed was dried at 100 °C over 48 h. Zinc (hydr)oxide was prepared in the same way, without the GO in $ZnCl_2$ solution. Prior to the chemical synthesis of ZnGO composites, the structure of the precursor materials was investigated. Some details on $Zn(OH)_2$ are discussed in Refs. 3 and 6. The structural details on the materials were studied using TEM, STEM, X-Ray analysis, and TPF imaging techniques.

a)Author to whom correspondence should be addressed. Electronic mail: ralfano@sci.ccny.cuny.edu. Tel.: 1-(212) 650 5531. Fax: 1-(212) 560 5530.

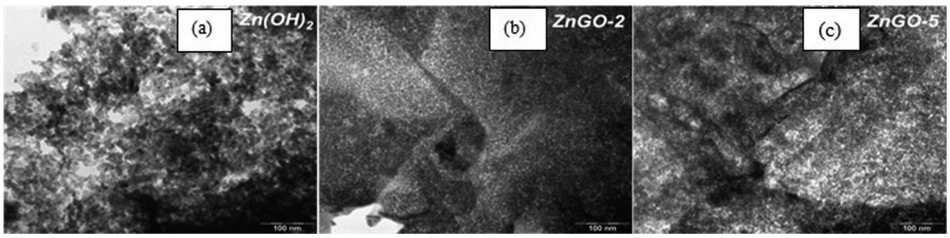

FIG. 1. TEM images for the (a) zinc (hydr)oxide $Zn(OH)_2$; (b) ZnGO-2; and (c) ZnGO-5.

III. CHARACTERIZATION OF $Zn(OH)_2$ AND ITS COMPOSITES

A. Structural characterization

TEM images, presented in Fig. 1, show that the texture $Zn(OH)_2$ consists of loosely attached, small irregular particles. In the micro/meso-porous composites, ZnGO-2 and ZnGO-5, the particles of the inorganic phases deposited on graphene sheet look smaller than those in $Zn(OH)_2$. STEM images of ZnGO-5 (Fig. 2) show more details on the dimensions of zinc species particles. With an increasing magnification, it is seen that the deposition of particles on graphene sheets as a first layer is followed by the subsequent deposition of particles of similar sizes (between 2 nm and 4 nm, as seen from the 12 nm × 12 nm image in Fig. 2). The measured surface areas of $Zn(OH)_2$, ZnGO-2, and ZnGO-5 are 76, 64, and 64 m^2/g,[3,6] respectively, and the total pore volume increases with an increase in the amount of GO present in the composites. The X-Ray diffraction patterns presented in Fig. 3 indicate that zinc hydroxide and zinc hydroxychloride, $Zn_5(OH)_8Cl_2$, are present in structure of ZnGO-5.[6] The latter species is the only crystalline phase detected in ZnGO-2. The presence of chloride introduces surface heterogeneity and it may affect the band gap. Interestingly, the zinc (hydr)oxide particle sizes calculated from X-ray diffraction patterns (Fig. 3) using Scherrer equation[6] are larger than those seen in STEM images and the same is true for all three materials (Table I). This may suggest that they exist as rods or oval particles. The results of Energy Dispersive X-ray (EDX) analysis indicate that much more zinc hydroxychloride is present in ZnGO-2 than in ZnGO-5. Moreover, the higher Zn/Cl ratio in the former sample than that in the detected $Zn_5(OH)_8Cl_2$ points out the presence of zinc hydroxide but it must be in an amorphous form or its particles are too small to be detected using X-ray diffraction. STEM aberration corrected[11] images were obtained using Nion Ultra-STEM-100, equipped with a cold field emission electron source and a corrector of 3rd and 5th order aberrations. The microscope was operated at 60 kV accelerating voltage, which is below the knock-on radiation damage threshold in graphene.

Light emitting regions and a network of pores of these composite materials are identified via a TPF imaging microscopy. TPF imaging identifies light emitting regions. It also identifies the pores and voids of samples. Using this imaging technique, particle size and distribution can be estimated. TPF imaging was performed with the Ultima Multi-Photon-Microscope (Olympus BX-51 of Prairie Tech. Inc., WI, USA). An excitation wavelength between 680 and 1080 nm was used to conduct TPF imaging. The samples, in particular, were excited with100-fs laser pulses at a wavelength of 790 nm using the Ti-Sapphire (Chameleon Ultra II laser, Coherent Inc.) laser, and the fluorescence emitted from the specimen was collected by the photomultiplier tubes (PMTs) after passing barrier filters (450–490 nm). The images (239.1 μm × 239.1 μm) produced on the screen (512 × 512 pixels) were recorded as shown in Fig. 4. Previous work,[12] particularly TPF images, reports that the average size (i.e., diameter) of micro/meso-pores were found to be ~11.94 ± 3.21 μm, ~17.83 ± 4.52 μm, and ~23.48 ± 5.18 μm for $Zn(OH)_2$, ZnGO-2, and ZnGO-5, respectively. These pores are suitable for incorporating ions, quantum dots, dye molecules, and other dopants.

B. Optical gaps characterization by absorption spectroscopy

In the absorption spectra, there appear several common features on the absorption edge commonly shown in amorphous, non-crystalline, and crystalline semiconductor materials.[13] The main features of the edges are direct edge and Urbach tail. The characteristic slope of the exponential part of the absorption edge, commonly referred as the Urbach edge, is found to be proportional to k_BT for temperatures above the Debye temperature[7] and is believed to be associated with disorder caused by thermal fluctuations of the electronic structures.[7,14,15] The weak portion of the absorption region, a measure of the width of the defect state, depends on the structural properties of the materials. The fundamental absorption edge follows the exponential law, and the absorption coefficient has the following spectral dependence:[16]

$$\alpha_1(E) = \alpha_o(E - E_g)^n, \quad (1)$$

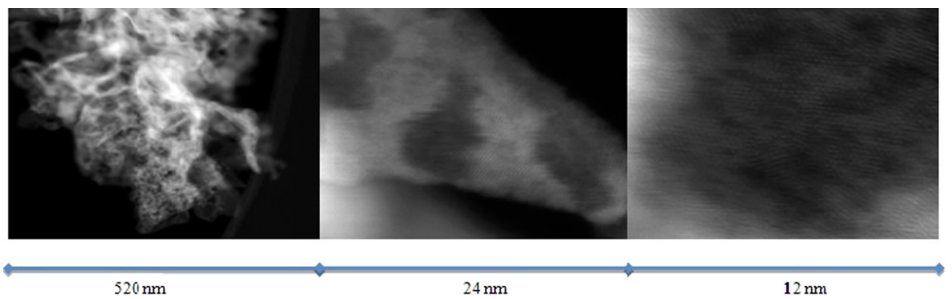

FIG. 2. STEM images of ZnGO-5 sample. The areas from left to right are: 520 × 520 nm, 24 nm × 24 nm, and 12 × 12 nm. The crystal lattice of small deposited particles of Zn $(OH)_2$ with sizes of 2 nm is seen on the GO layers.

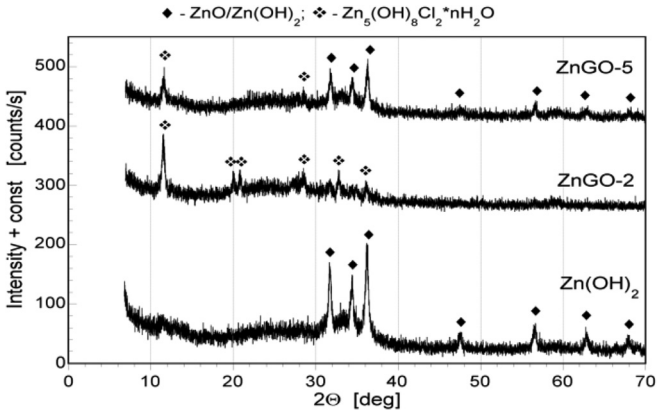

FIG. 3. X-ray patterns for three different materials: (a) $Zn(OH)_2$; (b) ZnGO-2; and (c) ZnGO-5.

TABLE I. Crystallographic structures, size of crystallites, and surface contents of Zn, O, and Cl in at. % evaluated using EDX.

Samples	Crystallographic structure detected	Crystal size Lc (nm)	Zn	O	Cl
$Zn(OH)_2$	$ZnO/Zn(OH)_2$	19.6	47.4	52.6	ND
ZnGO-2	$Zn_5(OH)_8Cl_2nH_2O$	20.3	54.0	24.2	8.2
ZnGO-5	$ZnO/Zn(OH)_2$	21.7	32	32.0	1.4
	$Zn_5(OH)_8Cl_2onH_2O$	17.2			

where $\alpha_1(E)$ is the absorption coefficient, $E = \hbar\omega$ is the photon energy, E_g is the band gap energy, α_0 characteristic parameter of the material, and finally, $n = 1/2$ for direct band gap and $n = 2$ for indirect band gap materials. The optical absorption edge in the exponential Urbach region, having its dependence on photon energy and temperature, can be given by[17,18]

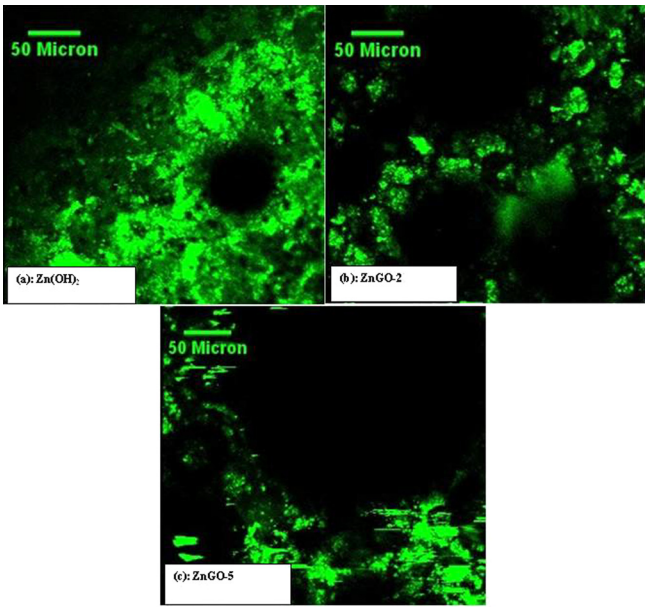

FIG. 4. TPF images showing voids and light-emitting regions [selected from partial parts of Fig. 2 in Ref. 12]: (a) A 2-D image for $Zn(OH)_2$ with the pore size ranging from 20 μm to 63 μm; (b) A 2-D image for ZnGO-2 with the pore size ranging from 25 μm to 255 μm; and (c) A 2-D image for ZnGO-5 with pore size ranging from 20 μm to 232 μm.

$$\alpha_2(E,T) = \alpha_g \exp\left(\frac{E - E_{op}}{E_u}\right), \tag{2}$$

where $\alpha_2(E,T)$ is the temperature dependent absorption coefficient. $E$is the photon energy (i.e., $E = \hbar\omega$); E_{op} and E_u are temperature-dependent fitting parameters,[18,19] where E_{op} is comparable to the band-gap energy ($E_{op} = E_g(T)$)[18] and E_u being proportional to k_BT in Urbach's original work.[19] Here, the optical band gap energy is defined as the energy at which the extrapolated absorption coefficient reaches α_g, which is one of the Urbach bundle convergence point coordinates.[17,18] Combining the two key processes for absorption makes use of Eqs. (1) and (2), a form that has been used for simulation for absorption vs. energy is given by

$$\alpha(E) = \alpha_1(E) + \alpha_2(E). \tag{3}$$

The diameter ($\sim 8 \pm 0.01$ mm) and thickness ($\sim 150 \pm 5$ μm) of the samples for absorption spectroscopy, fluorescence spectroscopy, and photocurrent experiment were measured by Accupro dial thickness gauge gage measurement tool. The absorption measurements were carried out at room temperature using Varian's Cary 500 Scan (UV-VIS-NIR) Spectrophotometer. A beam of light with a spectral range between 250 and 800 nm from a broad-band light source was passed through an aperture of 6 mm in diameter and was allowed to impinge upon the samples. The absorption started at 400 nm ($\sim$3.1 eV), as shown in Figs. 5(a)–5(c). A very good agreement is seen between the experimental data and the data obtained by a numerical method. Using the least square fitting technique for a third order polynomial function, this simulation method involved Eqs. (2) and (3) to find the optical band gap energy E_{op} and direct energy-gap energy E_g^D (Fig. 5(a)) and Urbach energy E_u. The energy gap values along with fitting parameters are listed in Table II.

The investigated materials are micro/meso-porous and they lack any long-range order and are considered to be amorphous. In characterizing optical band gap parameters of such materials, three (high, medium, and low) spectral regions have been identified. The absorption coefficient (i.e., $\alpha_0 = 330\ cm^{-1}$, $480\ cm^{-1}$, and $440\ cm^{-1}$) for the direct-gap region for the samples of $Zn(OH)_2$ and its composites ZnGO-2 and ZnGO-5, respectively, are estimated. Absorption-coefficient for one of the Urbach convergence point coordinates (i.e., $\alpha_g = 58\ cm^{-1}$,$130\ cm^{-1}$, and $140\ cm^{-1}$) for the Urbach tail region for the above-mentioned samples is also estimated. The absorption coefficient for the lowest region that depends on the structural properties of the materials is not reported here. The characteristic direct-gap energy, lying below the optical gap region, which depends on phonon beating, has been obtained after taking off the thermal energy contribution due to temperature fluctuation even at room temperature. The thermal fluctuations that are occurring even at the short-range orders are the basic attributes of these materials. The detailed analysis of the dependence of Urbach energy on various factors, such as, structural feature, aggregate state, crystal lattice dimensionality, types of phase transitions is beyond the scope of this paper. One more important point is that absorption coefficient below $10\ cm^{-1}$

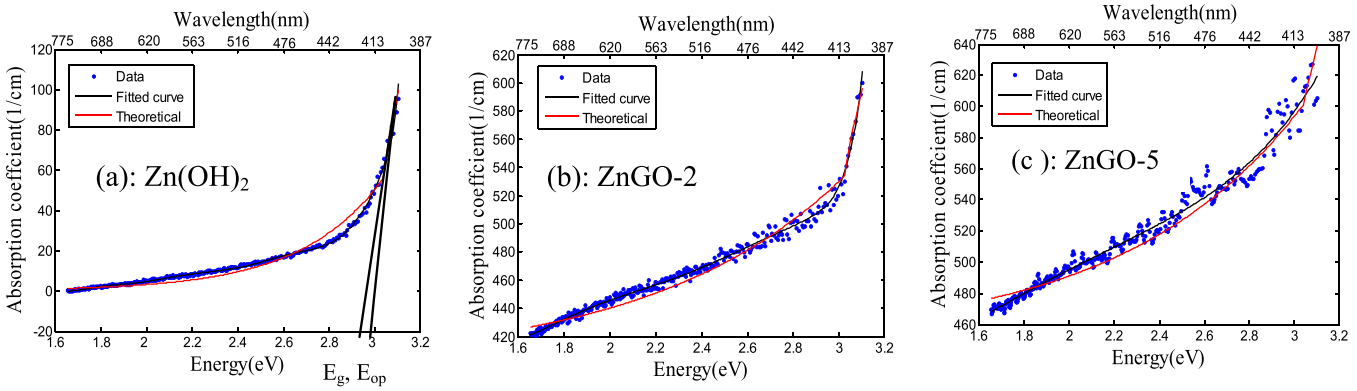

FIG. 5. Plots from absorption data for determining the band gap energies and absorption-coefficients for three different materials: (a) porous $Zn(OH)_2$; (b) composite ZnGO-2; and (c) composite ZnGO-5. In Fig. 5(a), the left vertically slanted line intersecting with horizontal (energy) axis denotes E_g and the right one intersecting the energy axis denotes E_{op}.

has not been included in the simulation scheme, because the data below those values are more sensitive to the approximations in the model calculations and uncertainties associated with the subtraction of the low-energy absorption.

C. Photoluminescence spectroscopy

In photoluminescence experiment, the samples were excited with energy above the optical band gap energy. This experiment exhibits both radiative and non-radiative relaxation. The photoluminescence experiments were carried out at room temperature using a Perkin-Elmer LS-50 fluorescence spectrometer. The samples were excited with a beam of light at 300 nm (~4.13 eV) and fluorescence was collected between 320 nm and 760 nm. The first peak, for $Zn(OH)_2$ sample, appears at 400 nm (~3.1 eV) and the highest intensity peak appears at around 420 nm (~2.95 eV), as shown in Fig. 6(a). The subsequent peaks visible on the spectrum are attributed to phonon assisted recombination at lower photon energy in regions where materials are more transparent as reported in case of some semiconductors.[7] It is recognized that there might be impurity-assisted non-radiative transitions for which band broadening can be attributed.[7] The optical band-gap energies for samples were found from using the following equation:

$$E_{op} = E_g^{PL} + 0.5k_BT. \quad (4)$$

The $E_g^{PL} = 2.93$ eV was obtained for $Zn(OH)_2$ after subtracting the contribution due to Boltzmann factor $(0.5k_BT)$ from optical band gap energy E_{op} (i.e., energy corresponding to the highest peak). Likewise, $E_g^{PL} = 2.87$ eV for ZnGO-2 and $E_g^{PL} = 2.84$ eV for ZnGO-5 were recorded. In Eq. (4), E_g^{PL} is the direct band-gap (i.e., minimum band-gap) energy and the full width at half maximum of the emission line is very close to the Boltzmann factor, k_BT.[20]

TABLE II. Band-gap energies (eV) and absorption coefficients (cm^{-1}) of three different materials obtained via absorption, photoluminescence, photocurrent techniques, and a numerical method.

Sample	Absorption	Photoluminescence	Photocurrent
$Zn(OH)_2$	$E_g^D = 2.97$		
	$E_{op} = 3.00$		
	$E_{ou} = 0.36$	$E_g^{PL} = 2.93$	$E_g^{PC} = 3.06$
	$\alpha_0 = 330$		
	$\alpha_g = 58$		
ZnGO-2	$E_g^D = 2.93$		
	$E_{op} = 2.95$		
	$E_{ou} = 0.85$	$E_g^{PL} = 2.87$	$E_g^{PC} = 2.88$
	$\alpha_0 = 480$		
	$\alpha_g = 130$		
ZnGO-5	$E_g^D = 2.84$		
	$E_{op} = 2.88$		
	$E_{ou} = 0.80$	$E_g^{PL} = 2.84$	$E_g^{PC} = 2.85$
	$\alpha_0 = 440$		
	$\alpha_g = 140$		

D. Photoconductivity spectroscopy

The photoconductivity experiments were carried out using a Triax 320 monochromator to select wavelength of light from a Quartz Tungsten Halogen Lamp in a wide spectrum range from 300 nm to 1200 nm. Photocurrent spectra were recorded by a SR 830-DSP Locking Amplifier. The light beam coming out from monochromator was focused onto an area in between electrodes over the samples. Lamp spectrum emerging from monochromator was measured by a UV enhanced silicon detector. A grating with blazing wavelength of 500 nm was used for all measurements. Figs. 7(a)–7(c) show photocurrent curves for all the three samples. All photocurrent spectra cover a spectral range from 300 nm to 800 nm. The photocurrent peak for $Zn(OH)_2$ appears at 405 nm (i.e., $E_g^{PC} = 3.06$ eV). Likewise, for ZnGO-2 and ZnGO-5, the photocurrent peaks appear at 430 nm (i.e., $E_g^{PC} = 2.88$ eV) and 435 nm (i.e., $E_g^{PC} = 2.85$ eV). The photocurrent measurement has been of very practical use, as this technique provides direct band gap energy for non-conducting materials and which has also been proven to be very useful information in designing the practical photo detectors. All band gap related energies and absorption coefficients, obtained by three optical characterization techniques, are compiled in Table II. These values show close correspondence with one another and with those values obtained by a numerical method.

IV. DISCUSSION

The data by optical characterization techniques and simulation methods suggest that the band gap narrowing occurs

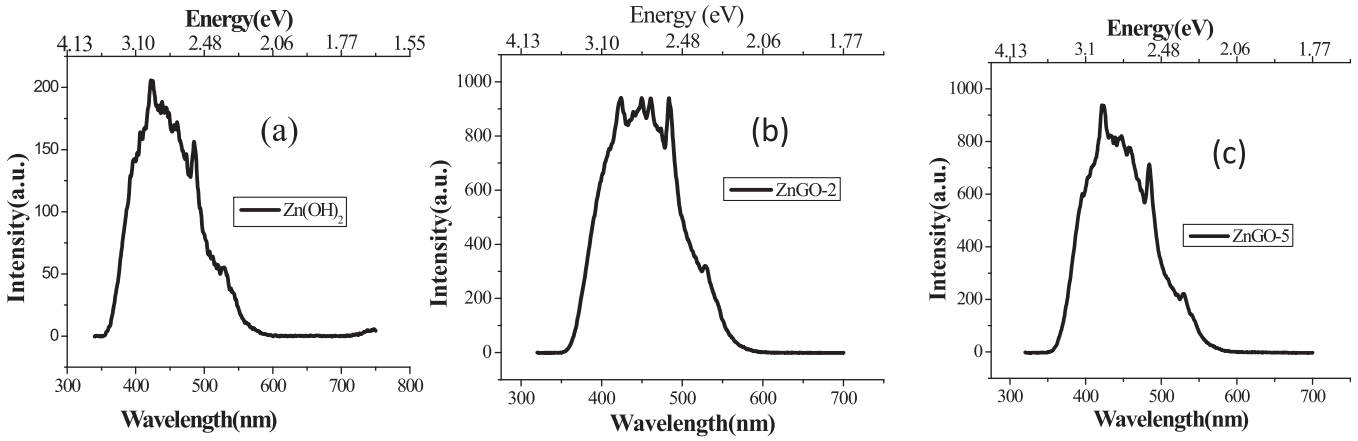

FIG. 6. Photoluminescence spectra of (a) $Zn(OH)_2$; (b) ZnGO-2; and (c)ZnGO-5.

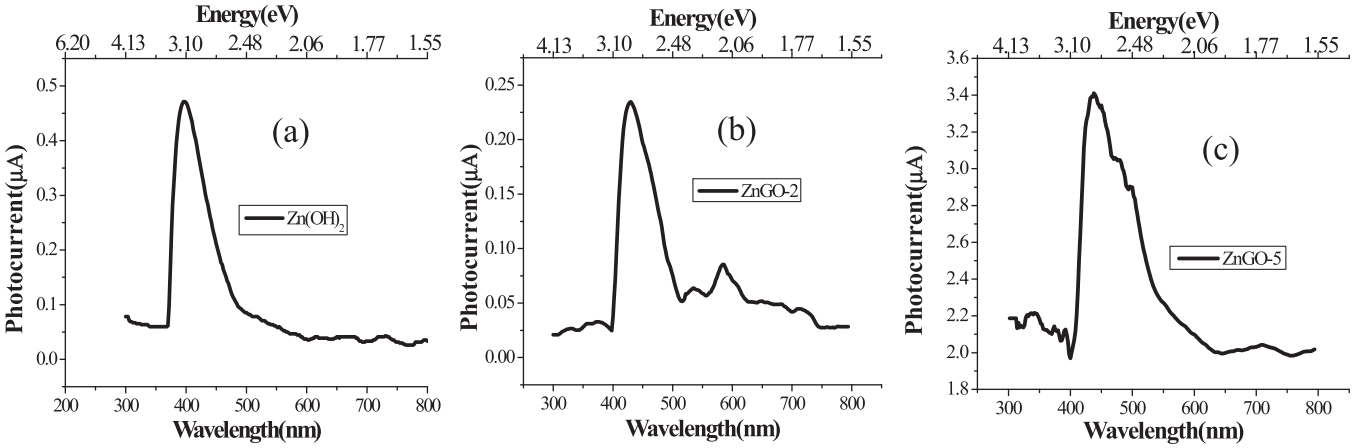

FIG. 7. Photocurrent spectra of (a) zinc (hydr)oxide $Zn(OH)_2$; and its composites (b) ZnGO-2 and (c) ZnGO-5.

for composites in comparison to zinc (hydr)oxide. Moreover, the energy-gap (~3.00 eV) of $Zn(OH)_2$ is found to be smaller than that of zinc oxide (~3.2 eV). The physics of band gap shrinkage in materials, ranging from nanocrystals to composites, has been investigated. The energy band gap narrowing has been attributed to the following phenomena: lattice disorder with the appearance of mid-gap electronic state, the electron-impurity interaction and Coulomb-interaction between carriers, nature and location of defects, the change in the nature and strength of the interaction potentials between donors and host materials, oxygen vacancies and interstitial sites, and disordered semiconductors.

Based on the surface properties of the studied materials,[3,6] we link a decrease in the energy gap in the composites with an increase in GO content, an increase in the amorphous-level of the zinc (hydr)oxide phase, relatively high level of impurity (chlorine), and the presence of hetero-junctions/bonds between the graphene layers and zinc (hydr)oxide lattice.[3] It has been shown that the bonds also increase the conductivity, which also suggests the phenomenon of energy-gap narrowing.

The defects in the lattice affect the interactions between electrons and phonons. Besides electron-phonon interaction effects, phonon-confinement due to addition of graphite-oxide phase and nano-sized particles of $Zn(OH)_2$ might have played a key role in downshifting the band gap energies in the composites. The larger size particles in the composites might contribute toward lower band gaps due to weaker confinement. The decrease in the band gap energy in $Zn(OH)_2$ compared to pure ZnO can be linked to the defects in the lattice of the material resulting in porous texture, and larger particles, accompanied by weaker confinement.

V. CONCLUSION

A new class of optical micro/meso-porous composites that exhibit band gap narrowing has been investigated. The synthesis schemes for $Zn(OH)_2$ and its composites, ZnGO-2 and ZnGO-5, are reported here. From band gap energy data, obtained by three optical spectroscopic techniques, the occurrence of band gap narrowing in composites is attributed to increase in the content of graphite oxide in composites. It has been postulated that the effects of particle size, defects, and graphene in composites might have played roles in decreasing band gap energies. The presented results on the photo spectral response from 350 nm to 600 nm open the possibility of engineering of these materials for myriad of applications, ranging

from sensors to energy-harvesting and energy conversion in hybrid solar cells. The use of quantum dots and dye molecules in these porous materials may increase solar energy conversion in a hybrid Grätzel-like solar cell.

ACKNOWLEDGMENTS

This work was supported at CCNY/CUNY by the Army Research Office grant W911NF-10-1-0030 and NSF Collaborative grant 1133112. The STEM research work was supported in part by Oak Ridge National Laboratory's Shared Research Equipment (ShaRE) User Program (J.C.I), which was sponsored by Scientific User Facility Division, Office of Basic Energy Sciences, U.S. Department of Energy; and CCNY's President Coico seed 2013 research program between faculty members (Professor Alfano and Professor Bandosz).

[1]J. T. Robinson, F. K. Perkins, E. S. Snow, Z. Wei, and P. E. Sheenhan, "Reduced graphene oxide molecular sensors," Nano Lett. **8**, 3137 (2008).
[2]M. Liang and L. Zhi, "Graphene-based electrode materials for rechargeable lithium batteries," J. Mater. Chem. **19**, 5871 (2009).
[3]M. Seredych, O. Mabayoje, M. M. Kolesnik, V. Krstic, and T. J. Bandosz, "Zinc (hydr)oxide/graphite based-phase composites: Effect of the carbonaceous phase on surface properties and enhancement in electrical conductivity," J. Mater. Chem. **22**, 7970 (2012).
[4]M. Seredych, O. Mabayoje, and T. Bandosz, "Visible-light-enhanced interactions of hydrogen sulfide with composites of zinc (oxy)hydroxide with graphite oxide and graphene," Langmuir **28**, 1337 (2012).
[5]M. Seredych, O. Mabayoje, and T. Bandosz, "Involvement of water and visible light in the enhancement in SO_2 adsorption at ambient conditions on the surface of zinc (hydr)oxide/graphite oxide composites," Chem. Eng. J.: Environ. **223**, 442 (2013).
[6]O. Mabayoje, M. Seredych, and T. J. Bandosz, "Reactive adsorption of hydrogen sulfide on visible light photoactive zinc (hydr)oxide/graphite oxide and zinc (hydr)oxychloride/graphite oxide composites," Appl. Catal., B **132–133**, 321 (2013).
[7]S. R. Johnson and T. Tiedje, "Temperature dependence of the Urbach edge in GaAs," J. Appl. Phys. **78**, 5609 (1995).
[8]S. Chen, J. Zhu, X. Wu, Q. Han, and X Wang, "Graphene oxide−MnO_2 nanocomposites for supercapacitors," ACS Nano **4**, 2822 (2010).
[9]H.-J. Shin, K. K. Sim, A. Benayad, S.-M. Moon, H. K. Park, I.-S. Jung, M. H. Jin, H.-K Jeong, J.-Y Choi, and Y. H. Lee, "Efficient reduction of graphite oxide by sodium borohydride and its effect on electrical conductance," Adv. Funct. Mater. **19**, 1987 (2009).
[10]W. S. Hummers and R. E. Offeman, "Preparation of graphite oxides," J. Am. Chem. Soc. **80**, 1339 (1958).
[11]O. L. Krivanek, G. J. Corbin, N. Dellby, B. F. Elston, R. J. Keyse, M. F. Murfitt, C. S. Own, Z. S. Szilagyi, and J. W. Woodruff, "An electron microscope for the aberration-corrected era," Ultramicroscopy **108**, 179 (2008).
[12]SM. Z. Islam, T. Gayen, A. Moussawi, L. Shi, M. Seredych, T. J. Bandosz, and R. Alfano, "Structural and optical characterization of $Zn(OH)_2$ and its composites with graphite oxides," Opt. Lett. **38**, 962 (2013).
[13]M. Kranjcec, I. P. Studenyak, and M. V. Kurik, "Urbach rule and disordering process in $CuP(S_{1-x}Se_x)Br_{1-y}I_y$ supersonic conductors," J. Phys. Chem. Solids **67**, 807 (2006).
[14]S. R. Johnson and T. Tiedje, "Temperature dependence of the Urbach edge in GaAs," J. Appl. Phys. **78**, 5609 (1995).
[15]K. Tanaka and S.-i. Nakayama, "Where is the mobility edge in amorphous semiconductors?," J. Optoelectron. Adv. Mater. **2**, 5 (2000).
[16]J. I. Pankov, *Optical Process in Semiconductor* (Dover Publications, Inc., NY, 1971), Chap. 3, p. 36.
[17]M. Kranjcec, I. P. Studenyak, and M. V. Kuric, "Specific features of the optical absorption edge anisotropy in $In_4(P_2S_6)_3$ layered crystals," J. Non-Cryst. Solids **355**, 54 (2009).
[18]C. H. Grein and S. John, "Temperature dependence of the Urbach optical absorption edge: A theory of multiple phonon absorption and emission sidebands," Phys. Rev. B **39**, 1140 (1989).
[19]S. John, C. Soukoulis, M. H. Cohen, and E. N. Economou, "Theory of electron band and the Urbach optical-absorption edge," Phys. Rev. Lett. **57**, 1777 (1986).
[20]M. Fox, *Optical Properties of Solids* (Oxford University Press, NY, 2010), Chap. 5, p. 121.